K. Stein
Department of Physics,
Bethel College,
St. Paul, MN 55112

T. Tezduyar
Mechanical Engineering,
Rice University,
MS 321,
Houston, TX 77005

R. Benney
Natick Soldier Center,
Natick, MA 01760

Mesh Moving Techniques for Fluid-Structure Interactions With Large Displacements

In computation of fluid-structure interactions, we use mesh update methods consisting of mesh-moving and remeshing-as-needed. When the geometries are complex and the structural displacements are large, it becomes even more important that the mesh moving techniques are designed with the objective to reduce the frequency of remeshing. To that end, we present here mesh moving techniques where the motion of the nodes is governed by the equations of elasticity, with selective treatment of mesh deformation based on element sizes as well as deformation modes in terms of shape and volume changes. We also present results from application of these techniques to a set of two-dimensional test cases. [DOI: 10.1115/1.1530635]

1 Introduction

Computation of flows with fluid-structure interactions was one of the objectives in development of the Deforming-Spatial-Domain/Stabilized Space-Time (DSD/SST) formulation, [1–3], for flows with moving boundaries and interfaces. This is an interface-tracking technique, and as such requires that the mesh be updated to track the moving interfaces as the spatial domain occupied by the fluid is varying (i.e., deforming) with respect to time. In computations with the arbitrary Lagrangian-Eulerian method, which is another interface-tracking method, one faces the same requirement. In general, mesh update consists of moving the mesh for as long as it is possible, and full or partial remeshing (i.e., generating a new set of elements, and sometimes also a new set of nodes) when the element distortion becomes too high.

As the mesh moves, the normal velocity of the mesh at the interface has to match the normal velocity of the fluid. With this condition met, our main objective in designing a mesh update technique becomes reducing the remeshing frequency. This is very important in three-dimensional computations with complex geometries, because remeshing in such cases typically requires calling an automatic mesh generator and projecting the solution from the old mesh to the new one. Both of these steps involve large computational costs.

In selecting a category of mesh moving techniques, geometric complexity is one of the major determining factors. Sometimes the overall problem geometry, including the interface geometry, is simple enough so that the mesh can be generated by a special-purpose mesh generation technique. In such cases, the mesh can be updated by using a special-mesh moving technique, without calling an automatic mesh generator and without solving any additional equations to determine the motion of the mesh. This approach involves virtually no mesh update cost, and one of its earliest examples, two-dimensional computation of sloshing in a laterally vibrating container, can be found in [1].

In most practical problems, such as the parachute fluid-structure interactions, the overall problem geometry would be too complex to use a special-purpose mesh generation technique. The mesh produced with an automatic mesh generator would require an au-

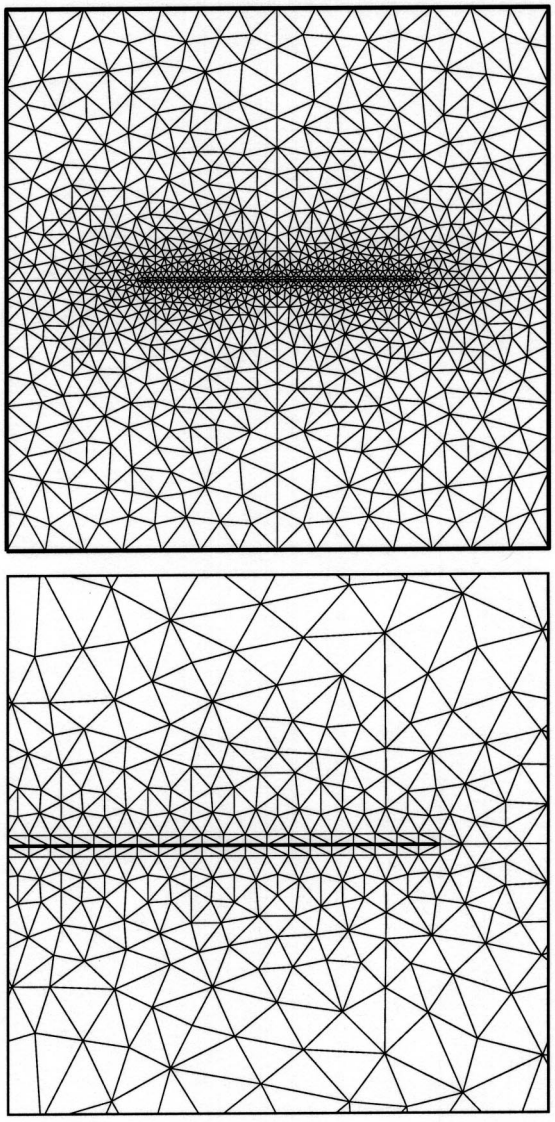

Fig. 1 Two-dimensional test mesh

Contributed by the Applied Mechanics Division of THE AMERICAN SOCIETY OF MECHANICAL ENGINEERS for publication in the ASME JOURNAL OF APPLIED MECHANICS. Manuscript received by the ASME Applied Mechanics Division, Dec. 4, 2001; final revision, Mar. 4, 2002. Associate Editor: L. T. Wheeler. Discussion on the paper should be addressed to the Editor, Prof. Robert M. McMeeking, Department of Mechanical and Environmental Engineering University of California–Santa Barbara, Santa Barbara, CA 93106-5070, and will be accepted until four months after final publication of the paper itself in the ASME JOURNAL OF APPLIED MECHANICS.

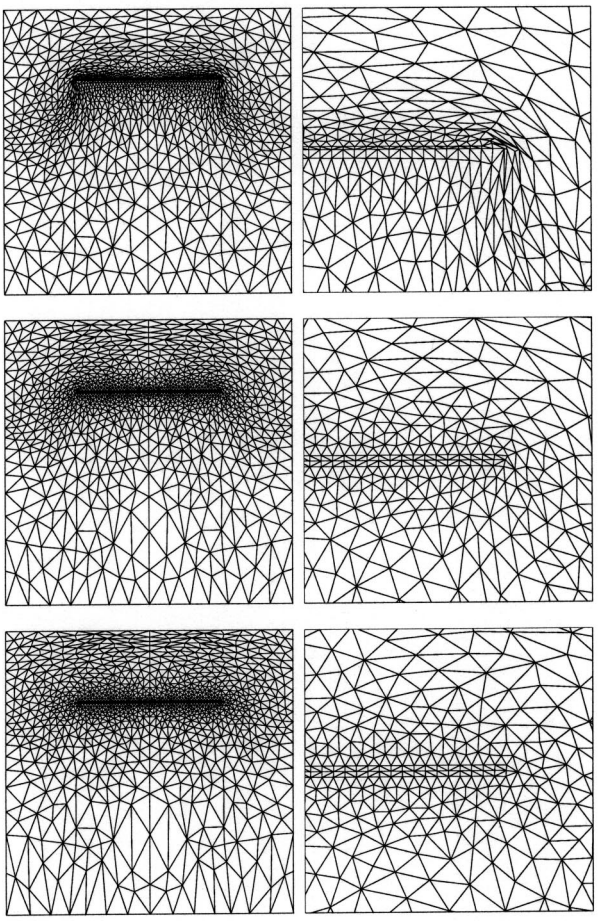

Fig. 2 Translation tests. Deformed mesh for $\chi = 0.0, 1.0, 2.0$.

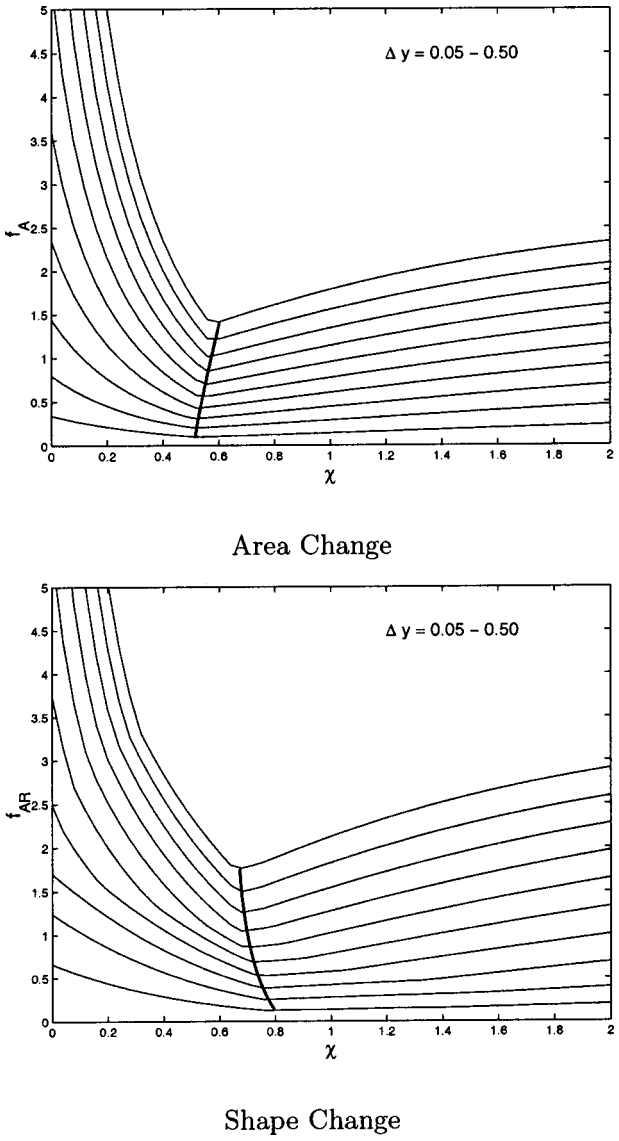

Fig. 3 Translation tests. Mesh quality as function of stiffening power.

tomatic mesh moving technique. We use the technique introduced in [4], where the motion of the nodes is governed by the equations of elasticity, and the mesh deformation is dealt with selectively based on the sizes of the elements and also the deformation modes in terms of shape and volume changes. The motion of the internal nodes is determined by solving these additional equations. As boundary condition, the motion of the nodes at the interfaces is specified to match the normal velocity of the fluid at the interface. Mesh moving techniques with comparable features were introduced in [5].

In the technique introduced in [4], selective treatment of the mesh deformation based on shape and volume changes is implemented by adjusting the relative values of the Lamé constants of the elasticity equations. The objective would be to stiffen the mesh against shape changes more than we stiffen it against volume changes. Selective treatment based on element sizes, on the other hand, is implemented by simply altering the way we account for the Jacobian of the transformation from the element domain to the physical domain. In this case, we would like the smaller elements to be stiffened more than the larger ones.

In this paper, we augment the method described in [4] to a more extensive kind, where we introduce a stiffening power that determines the degree by which the smaller elements are rendered stiffer than the larger ones. When the stiffening power is set to zero, the method reduces back to an elasticity model with no Jacobian-based stiffening. When it is set to one, the method is identical to the one introduced in [4]. Our studies here include seeking optimum values of this stiffening power with the objective of reducing the deformation of the smaller elements, typically placed near solid surfaces. In this context, by varying the stiffening power, we generate a family of mesh moving techniques, and test these techniques on fluid meshes where the structure undergoes three different types of prescribed motion or deformation.

2 Mesh Moving Model

2.1 Equations of Linear Elasticity. Let $\Omega \subset \mathbb{R}^{n_{sd}}$ be the spatial domain bounded by Γ, where n_{sd} is the number of space dimensions. Corresponding to the Dirichlet and Neumann-type boundary conditions, the boundary Γ is composed of Γ_g and Γ_h. The equations governing the displacement of the internal nodes can then be written as

$$\nabla \cdot \boldsymbol{\sigma} + \mathbf{f} = \mathbf{0} \quad \text{on } \Omega, \tag{1}$$

where $\boldsymbol{\sigma}$ is the Cauchy stress tensor and $\mathbf{f}$ is the external force. For linear elasticity, $\boldsymbol{\sigma}$ is defined as

$$\boldsymbol{\sigma} = \lambda \, \mathrm{tr}(\boldsymbol{\varepsilon}(\mathbf{y}))\mathbf{I} + 2\mu\boldsymbol{\varepsilon}(\mathbf{y}), \tag{2}$$

where $\mathbf{y}$ is the displacement, tr( ) is the trace operator, λ and μ are the Lamé constants, $\mathbf{I}$ is the identity tensor, and $\boldsymbol{\varepsilon}(\mathbf{y})$ is the strain tensor:

$$\boldsymbol{\varepsilon}(\mathbf{y}) = \frac{1}{2}(\nabla \mathbf{y} + (\nabla \mathbf{y})^{\mathrm{T}}). \tag{3}$$

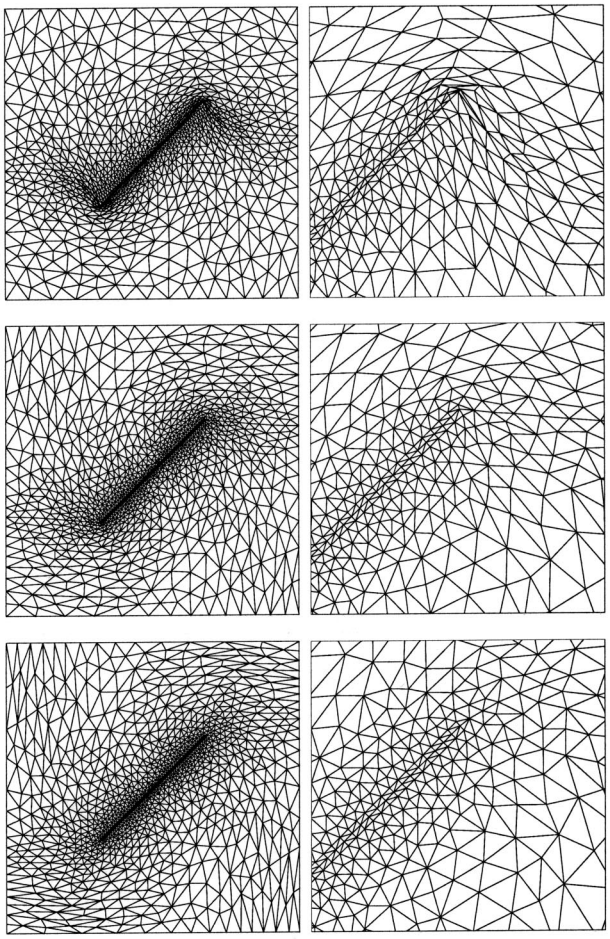

Fig. 4 Rotation tests. Deformed mesh for $\chi = 0.0, 1.0, 2.0$.

The Dirichlet and Neumann-type boundary conditions are represented as

$$\mathbf{y} = \mathbf{g} \quad \text{on } \Gamma_g,$$

$$\mathbf{n} \cdot \boldsymbol{\sigma} = \mathbf{h} \quad \text{on } \Gamma_h. \tag{4}$$

2.2 Finite Element Formulation. In writing the finite element formulation for Eq. (1), we first define the finite element trial and test function spaces $\mathcal{S}^h$ and $\mathcal{V}^h$:

$$\mathcal{S}^h = \{\mathbf{y}^h | \mathbf{y}^h \in [H^{1h}(\Omega)]^{n_{sd}}, \mathbf{y}^h \doteq \mathbf{g}^h \quad \text{on } \Gamma_g\}, \tag{5}$$

$$\mathcal{V}^h = \{\mathbf{w}^h | \mathbf{w}^h \in [H^{1h}(\Omega)]^{n_{sd}}, \mathbf{w}^h \doteq \mathbf{0} \quad \text{on } \Gamma_g\}. \tag{6}$$

Here, $H^{1h}(\Omega)$ is the finite-dimensional function space over Ω. The finite element formulation for Eq. (1) is then written as follows: find $\mathbf{y}^h \in \mathcal{S}^h$ such that $\forall \mathbf{w}^h \in \mathcal{V}^h$

$$\int_\Omega \boldsymbol{\varepsilon}(\mathbf{w}^h) : \boldsymbol{\sigma}(\mathbf{y}^h) d\Omega - \int_\Omega \mathbf{w}^h \cdot \mathbf{f} d\Omega = \int_{\Gamma_h} \mathbf{w}^h \cdot \mathbf{h} d\Gamma. \tag{7}$$

By assigning appropriate values to the ratio λ/μ, we can produce to a certain extent the desired effect in terms of volume and shape changes for the elements during the mesh motion. This approach becomes more clear if we rewrite the term that generates the stiffness matrix as

$$\boldsymbol{\varepsilon}(\mathbf{w}^h) : \boldsymbol{\sigma}(\mathbf{y}^h)$$

$$= \left(\lambda + \frac{2}{n_{sd}}\mu\right) \mathrm{tr}(\boldsymbol{\varepsilon}(\mathbf{w}^h)) \mathrm{tr}(\boldsymbol{\varepsilon}(\mathbf{y}^h)) + 2\mu \boldsymbol{\varepsilon}'(\mathbf{w}^h) : \boldsymbol{\varepsilon}'(\mathbf{y}^h), \tag{8}$$

where

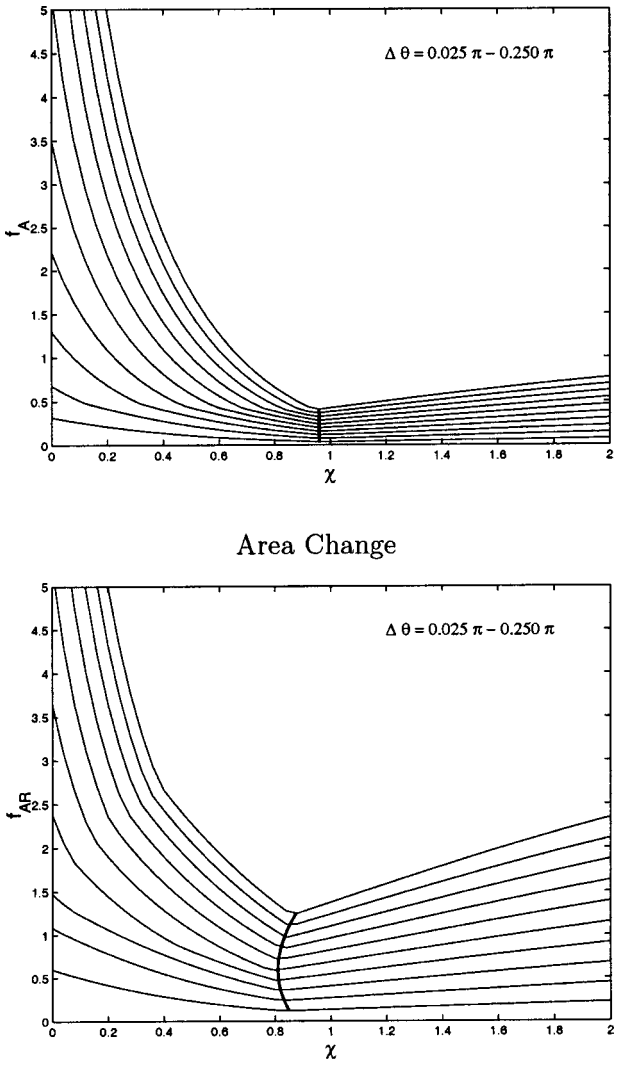

Fig. 5 Rotation tests. Mesh quality as function of stiffening power.

$$\boldsymbol{\varepsilon}'(\mathbf{y}^h) = \boldsymbol{\varepsilon}(\mathbf{y}^h) - \frac{1}{n_{sd}} \mathrm{tr}(\boldsymbol{\varepsilon}(\mathbf{y}^h)) \mathbf{I}. \tag{9}$$

The two terms on the right-hand side of Eq. (8) can be recognized as those corresponding, respectively, to the volume and shape change components of the stiffness matrix. In this context, the relative values of $(\lambda + 2/n_{sd}\,\mu)$ and 2μ can be adjusted to produce to a certain extent the desired effect in terms of stiffening the mesh against volume or shape changes.

Although a selective treatment of the mesh deformation can be incorporated also into the force vector $\mathbf{f}$ by providing an appropriate definition for the forcing function, in our case we set it equal to zero.

2.3 Jacobian Options. A selective treatment of the mesh deformation based on the element sizes can be implemented by simply altering the way we account for the Jacobian of the transformation from the element domain to the physical domain. This method was first introduced in [4], where the Jacobian is dropped from the finite element formulation, resulting in the smaller elements being stiffened more than the larger ones. Here we augment

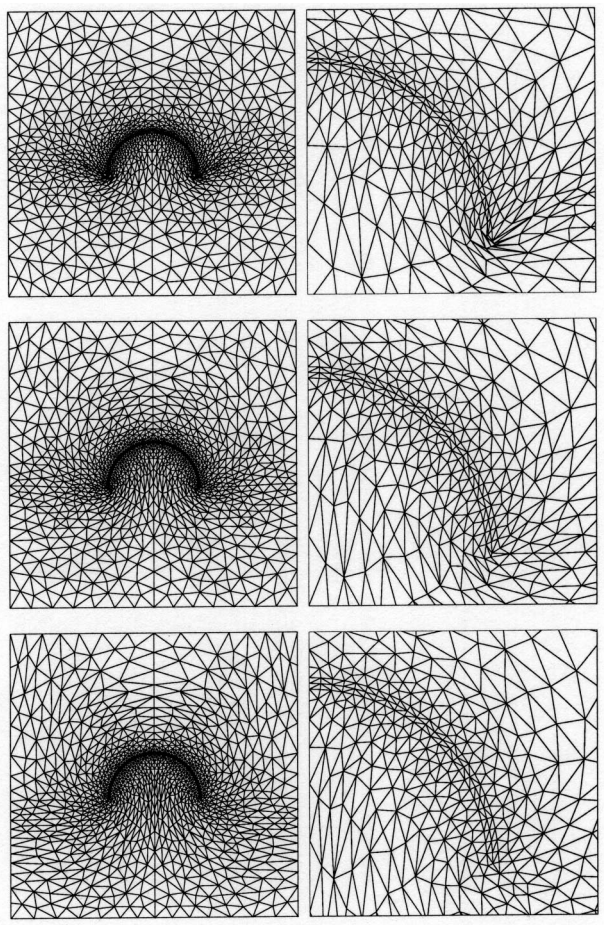

Fig. 6 Bending tests. Deformed mesh for $\chi = 0.0, 1.0, 2.0$.

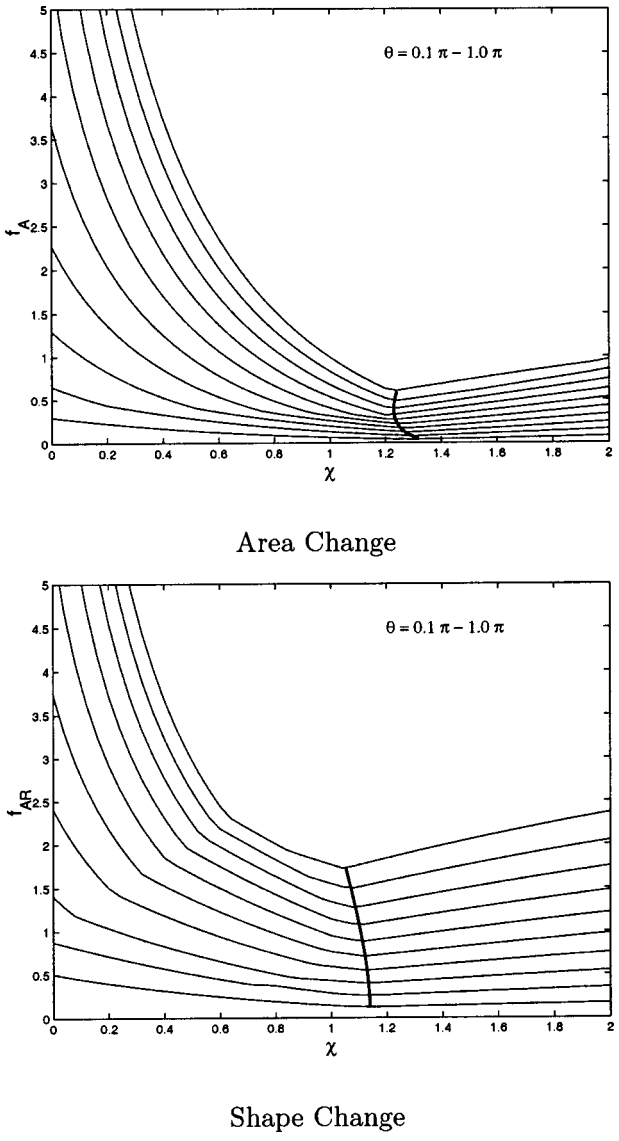

Fig. 7 Bending tests. Mesh quality as function of stiffening power.

that method to a more extensive kind. To describe this approach, we first write the global integrals generated by the terms in Eq. (8) as

$$\int_{\Omega} [\ \dots\ ] d\Omega = \sum_{e} \int_{\Xi} [\ \dots\ ]^e J^e d\Xi, \tag{10}$$

where $[\ \dots\ ]$ symbolically represents what is being integrated, Ξ is the finite element (parent) domain, and the Jacobian for element e is defined as

$$J^e = \det\left(\frac{\partial \mathbf{x}}{\partial \boldsymbol{\xi}}\right)^e. \tag{11}$$

Here $\mathbf{x}$ represents the physical coordinates, and $\boldsymbol{\xi}$ represents the element (local) coordinates.

We alter the way we account for the Jacobian as follows:

$$\int_{\Xi} [\ \dots\ ]^e J^e d\Xi \mapsto \int_{\Xi} [\ \dots\ ]^e J^e \left(\frac{J^0}{J^e}\right)^{\chi} d\Xi, \tag{12}$$

where χ, a non-negative number, is the stiffening power, and J^0, an arbitrary scaling parameter, is inserted into the formulation to make the alteration dimensionally consistent. With $\chi = 0.0$, the method reduces back to an elasticity model with no Jacobian-based stiffening. With $\chi = 1.0$, the method is identical to the one first introduced in [4]. In the general case of $\chi \neq 1.0$, the method stiffens each element by a factor of $(J^e)^{-\chi}$, and χ determines the degree by which the smaller elements are rendered stiffer than the larger ones.

3 Test Cases

The test cases are all based on a two-dimensional unstructured mesh consisting of triangular elements and an embedded structure with zero thickness. The mesh spans a region of $|x| \leq 1.0$ and $|y| \leq 1.0$. The structure spans $y = 0.0$ and $|x| \leq 0.5$. A thin layer of elements (with $\ell_y = 0.01$) are placed along both sides of the structure, with 50 element edges along the structure (i.e., $\ell_x = 0.02$). Figure 1 shows the mesh and its close up view near the structure.

The test cases involve three different types of prescribed motion or deformation for the structure: rigid-body translation in the y-direction, rigid-body rotation about the origin, and prescribed bending. In the case of prescribed bending, the structure deforms from a line to a circular arc, with no stretch in the structure and no net vertical or horizontal displacement. The tests are carried out with the Jacobian-based stiffening technique defined by Eq. (12), where χ ranges from 0.0 (no stiffening) to 2.0.

3.1 General Test Conditions and Mesh Quality Measures

In all test cases the maximum displacement or deformation is reached over 50 increments. The mesh over which the elasticity equations are solved is updated at each increment. This update is based on the displacements calculated over the current mesh that

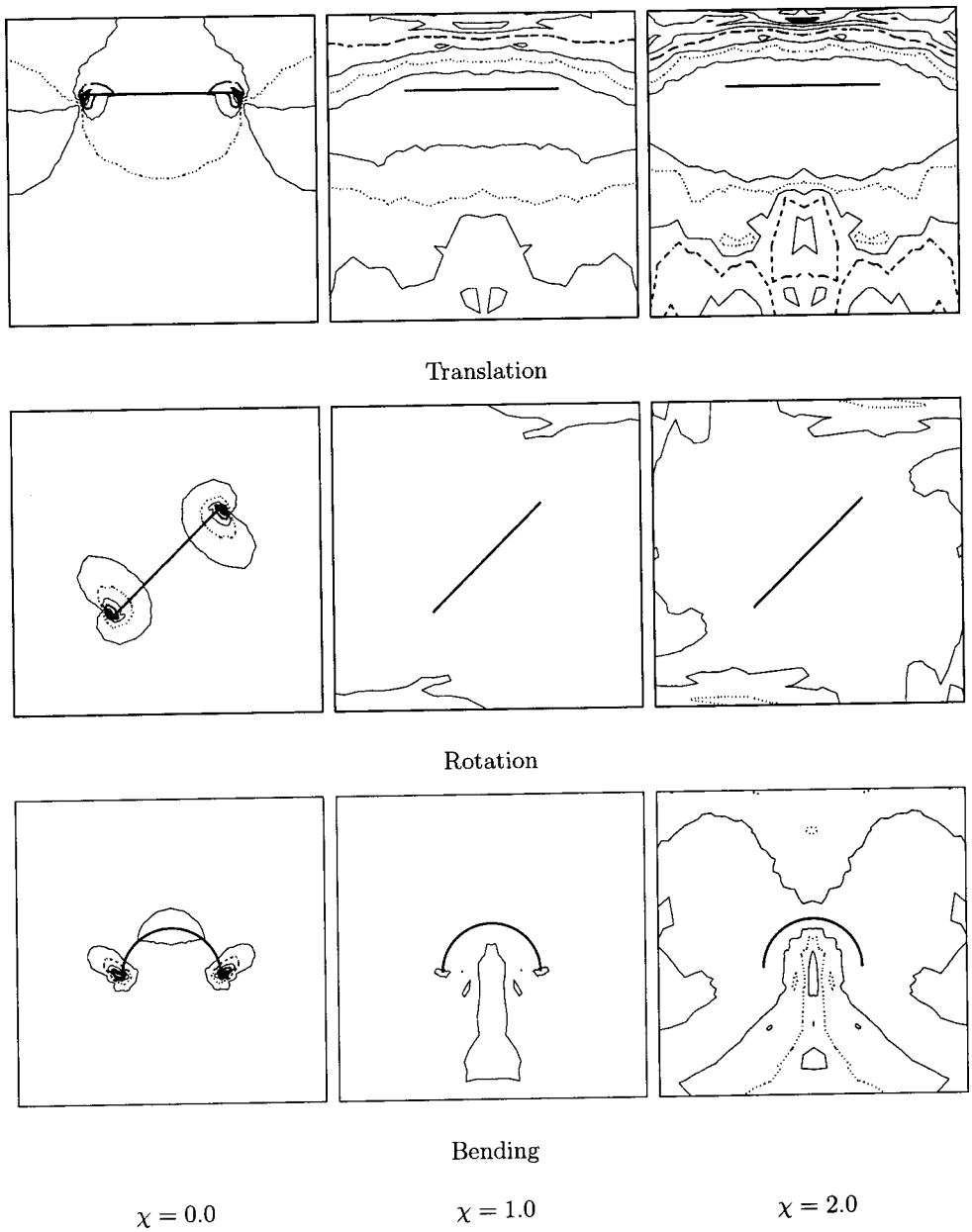

Fig. 8 Element area change (f_A^e)

has been selectively stiffened. That way, the element Jacobians used in stiffening are updated every time the mesh deforms. As a result, the most current size of an element is used in determining how much it is stiffened. Also as a result, as an element approaches a tangled state, its Jacobian approaches zero, and its stiffening becomes very large.

To evaluate the effectiveness of different mesh moving techniques, two measures of mesh quality are defined based on those used in [6]. They are *element area change* (f_A^e) and *element shape change* (f_{AR}^e):

$$f_A^e = \left| \log\left(\frac{A^e}{A_o^e} \right) / \log(2.0) \right|, \tag{13}$$

$$f_{AR}^e = \left| \log\left(\frac{AR^e}{AR_o^e} \right) / \log(2.0) \right|. \tag{14}$$

Here subscript "*o*" refers to the undeformed mesh (i.e., the mesh obtained after the last remesh) and AR^e is the element aspect ratio, defined as

$$AR^e = \frac{(l^e{}_{\max})^2}{A^e}, \tag{15}$$

where $l^e{}_{\max}$ is the maximum edge length for element e. For a given mesh, global area and shape changes (f_A and f_{AR}) are defined to be the maximum values of the element area and shape changes, respectively.

3.2 Test Results. In the translation tests, the prescribed translation is in the y-direction, with the displacement magnitudes ranging from $\Delta y = 0.05$ to 0.5. Figure 2 shows the deformed mesh for the maximum translation of $\Delta y = 0.5$. It is evident that the small elements near the structure respond poorly for $\chi = 0.0$, re-

sulting in severe stretching of the row of elements adjacent to the structure, and tangling of elements near the structure tips. For $\chi = 1.0$ and $\chi = 2.0$, the small elements near the structure experience no tangling and significantly less deformation. For $\chi = 2.0$, the small elements near the structure undergo almost rigid-body motion. However, the behavior of the larger elements deteriorates as the smaller elements are stiffened. This is most apparent for $\chi = 2.0$ where the larger element tangle near the upper boundary of the mesh. Figure 3 shows the values of f_A and f_{AR} as functions of χ and for different magnitudes of translation. The bold curve crossing the contours denotes the value of χ that results in minimum global mesh deformation. For example, for a displacement of 0.05 the optimal value of f_A is obtained when χ is approximately 0.5. For larger displacements, the optimal value of χ is slightly greater. The optimal value of f_{AR} is obtained at $\chi \approx 0.8$ for a displacement of 0.05 and at $\chi \approx 0.7$ for a displacement of 0.5.

In the rotation tests, the rotation magnitudes range from $\Delta\theta = 0.025\pi$ to 0.25π. For $\chi = 0.0$ the mesh experiences significant stretching and tangling near the structure tips. No tangling is seen for the cases with element stiffening, but for $\chi = 2.0$ the large elements near the outer boundaries experience significant distortion. Figure 4 shows the deformed mesh for the maximum rotation of $\pi/4$. Figure 5 shows the values of f_A and f_{AR} as functions of χ and for different magnitudes of rotation. The minimum deformation of the mesh is seen for values of χ around 0.8. The mesh quality deteriorates more rapidly as χ decreases from 1.0 than when χ increases from 1.0.

In the bending tests, the bending magnitudes range from $\theta = 0.1\pi$ to π, where θ denotes the arc length (in radians) for the deformed structure. Figure 6 shows the deformed mesh when the structure bends to a half-circle (i.e., $\theta = \pi$). For $\chi = 0.0$, we see tangling near the structure tips. As the element stiffening increases, tangling at the tips disappears, but severe element distortion arises in the interiors. Figure 7 shows the values of f_A and f_{AR} as functions of χ and for different magnitudes of prescribed bending. The minimum deformation of the mesh is seen for values of χ around 1.1.

Figure 8 shows, for different deformation modes, the contours of f_A^e for stiffening power of $\chi = 0.0$, 1.0, and 2.0. The contours corresponding to $f_A^e = 0.5$, 1.0, and 2.0 are denoted with dotted, dashed, and bold lines, respectively.

4 Concluding Remarks

We have presented automatic mesh moving techniques for fluid-structure interactions with large displacements. In these techniques, the motion of the nodes is governed by the equations of elasticity, and deformation of the elements are treated selectively based on element sizes as well as deformation modes in terms of shape and volume changes. Smaller elements, typically placed near solid surfaces, are stiffened more than the larger ones. This is implemented by altering the way we account for the Jacobian of the transformation from the element domain to the physical domain. The degree by which the smaller elements are stiffened more than the larger ones is determined by a stiffening power introduced into the formulation. When the stiffening power is set to zero, the method reduces back to a model with no Jacobian-based stiffening. The two-dimensional test cases we presented here for three different structural deformation modes show that the stiffening power approach substantially improves the deformed mesh quality near the solid surfaces, even when the displacements are large. The test cases also show that the optimal stiffening power is somewhat problem-dependent. It is higher for the bending tests ($\chi \approx 1.1$) than it is for the rotation ($\chi \approx 0.8$) and translation ($\chi \approx 0.7$) tests.

Acknowledgment

The work reported in this paper was partially sponsored by NASA JSC and by the Natick Soldier Center.

References

[1] Tezduyar, T. E., 1991, "Stabilized Finite Element Formulations for Incompressible Flow Computations," Adv. Appl. Mech., **28**, pp. 1–44.

[2] Tezduyar, T. E., Behr, M., and Liou, J., 1992, "A New Strategy for Finite Element Computations Involving Moving Boundaries and Interfaces—The Deforming-Spatial-Domain/Space-Time Procedure: I. The Concept and the Preliminary Tests," Comput. Methods Appl. Mech. Eng., **94**, pp. 339–351.

[3] Tezduyar, T. E., Behr, M., Mittal, S., and Liou, J., 1992, "A New Strategy for Finite Element Computations Involving Moving Boundaries and Interfaces—The Deforming-Spatial-Domain/Space-Time Procedure: II. Computation of Free-Surface Flows, Two-Liquid Flows, and Flows With Drifting Cylinders," Comput. Methods Appl. Mech. Eng., **94**, pp. 353–371.

[4] Tezduyar, T. E., Behr, M., Mittal, S., and Johnson, A. A., 1992, "Computation of Unsteady Incompressible Flows With the Finite Element Methods—Space-Time Formulations, Iterative Strategies and Massively Parallel Implementations," *New Methods in Transient Analysis*, P. Smolinski, W. K. Liu, G. Hulbert, and K. Tamma, eds., ASME, New York, AMD-Vol. 143, pp. 7–24.

[5] Masud, A., and Hughes, T. J. R., 1997, "A Space-Time Galerkin/Least-Squares Finite Element Formulation of the Navier-Stokes Equations for Moving Domain Problems," Comput. Methods Appl. Mech. Eng., **146**, pp. 91–126.

[6] Johnson, A. A., and Tezduyar, T. E., 1996, "Simulation of Multiple Spheres Falling in a Liquid-Filled Tube," Comput. Methods Appl. Mech. Eng., **134**, pp. 351–373.